Time-dependent screening effects in ion-atom collisions with many active electrons

T. Kirchner,[1] M. Horbatsch,[1] H. J. Lüdde,[2] and R. M. Dreizler[2]
[1]*Department of Physics and Astronomy, York University, Toronto, Ontario, Canada M3J 1P3*
[2]*Institut für Theoretische Physik, Universität Frankfurt, Robert-Mayer-Straße 8, D-60054 Frankfurt/Main, Germany*
(Received 14 May 2000; published 11 September 2000)

Ionization and electron transfer in collisions of bare ions from neutral target atoms with many active electrons are investigated within the independent particle model. We propose a simple model for the inclusion of time-dependent screening effects and discuss the question of how to analyze the solutions of the single-particle equations in order to avoid fluctuating transition probabilities, which normally occur when the effective mean-field potential depends on the propagated orbitals. The basis generator method is used to solve the single-particle equations for the $He^{2+}+Ne$ collision system in the energy range of 5 to 1000 keV/amu. It is shown that time-dependent screening effects reduce the cross sections for ionization and capture at low and intermediate impact energies significantly. Good overall agreement with experimental data is found except for the higher final charge states of the target ion.

PACS number(s): 34.10.+x, 34.50.Fa, 34.70.+e

I. INTRODUCTION

The quantum-mechanical description of ion-atom collisions which involve many interacting electrons remains an open problem in the theory of atomic collision processes, as the solution of the many-electron time-dependent Schrödinger (or Dirac) equation is far beyond present computational capabilities for most situations of interest. In fact, calculations which account for the correlated motion of the electrons have been mostly restricted to the two-electron problem [1], or to very low projectile energies, where electron capture is the dominant reaction channel and the many-electron wave function can be expanded in terms of a few molecular states [2]. At higher impact energies, the coupling to the continuum cannot be neglected and nonperturbative techniques to describe the competition between excitation, capture, and ionization processes are needed. Only at sufficiently high impact energies and for sufficiently low projectile charges do the different channels decouple, and perturbative methods can be applied. The field has been reviewed, e.g., in Ref. [3].

In recent publications we demonstrated that a large number of one- and two-electron processes in proton and antiproton collisions with many-electron target atoms can be successfully calculated over a broad range of impact energies in the framework of the independent particle model (IPM) with a frozen target potential that accounts accurately for electronic exchange effects [4–7]. Atomic potentials with this property were obtained from the exchange-only optimized potential method (OPM) [8]. Less convincing results were found for the collision calculation when the Latter-corrected local density approximation or Hartree-Fock-Slater potentials were used.

An important prerequisite for these studies was the development of the basis generator method (BGM) [9] for the solution of the effective single-particle time-dependent Schrödinger equations for all initially occupied orbitals. The BGM provides a representation of the electronic state vector during the collision in terms of dynamically adapted basis functions and has been shown to give accurate results for target excitation, electron capture, and total ionization cross sections for a variety of collision systems over a broad range of impact energies [6,7,10]. Despite the successful calculation of one- and two-electron processes, our work indicated that *multiple*-electron transitions at low and intermediate impact energies cannot be described satisfactorily in the framework of the IPM with a frozen target potential. Therefore, it is of interest to investigate to which extent the description can be improved within the IPM, if one goes beyond the frozen potential approximation and accounts for time-dependent screening effects. This task poses the two following major problems.

(1) The computational costs increase tremendously, when time-dependent screening effects are included on a microscopic level, as, e.g., within the time-dependent Hartree Fock (TDHF) theory [11], or within approximate schemes of time-dependent density functional theory (TDDFT) [12]. As a consequence, such calculations have been performed only rarely for ion-atom collision problems and were restricted to specific situations. Most of them concentrated on electron capture [13–15] or excitation [16] in (effective) two-electron scattering systems and relied on the TDHF approximation or a relativistic extension [17]. In a recent work, the time-dependent local density approximation was used to calculate charge transfer cross sections in $Ar^{8+}+Ar$ collisions [18]. The only calculation that included ionization processes was of a qualitative nature as it was performed in the so-called axial decoupling approximation, in which the rotational invariance of the wavefunction with respect to the internuclear axis was assumed [19].

(2) The nonlinearity of the single-particle Hamiltonian that includes time-dependent screening effects causes fundamental theoretical problems, such as the loss of the superposition principle in the equations of motion. As a result one obtains fluctuating transition probabilities when analyzing the solution with respect to eigenfunctions of the static asymptotic Hamiltonian. This so-called TDHF projection problem was observed in several calculations [16,20] and was discussed extensively in the context of nuclear reactions

[21]. To our knowledge no general solution has been found so far.

In this paper, we investigate the role of time-dependent screening effects in ion-atom collisions on the basis of a relatively simple model, which does not increase the computational cost significantly compared to a calculation with a frozen target potential. Furthermore, the projection problem can be fully understood and solved for this model, and stable transition probabilities are obtained for all channels. We present results for ionization and capture in the collision system $He^{2+}+Ne$, which has been investigated experimentally over a broad range of impact energies some time ago [22–24]. Very few theoretical results exist for this system [5,25].

The layout of the paper is as follows. We discuss our model for time-dependent screening effects and the projection problem in Sec. II. In Sec. III, some technical aspects of our calculations are summarized. Results for $He^{2+}+Ne$ collisions are presented in Sec. IV. We start with a discussion of net electron loss, capture and ionization in Sec. IV A, and compare cross sections for specific final charge states of the ions with experimental data in Sec. IV B. Our results are summarized in Sec. V. Atomic units ($\hbar=m_e=e=1$) are used throughout.

II. IPM DESCRIPTION OF ION-ATOM COLLISIONS WITH A TIME-DEPENDENT SCREENING POTENTIAL

Within the IPM description of the non-relativistic many-electron collision system the task is to solve a set of time-dependent Schrödinger-type equations for the initially occupied orbitals

$$i\partial_t\psi_i(\mathbf{r},t)=\hat{h}(t)\psi_i(\mathbf{r},t),\quad i=1,\ldots,N \tag{1}$$

with the Hamiltonian

$$\hat{h}(t)=-\frac{1}{2}\Delta-\frac{Q_T}{r}-\frac{Q_P}{|\mathbf{r}-\mathbf{R}(t)|}+v_{ee}(\mathbf{r},t). \tag{2}$$

Here, Q_T and Q_P denote the charges of the target and projectile nuclei, respectively, where the latter is assumed to move along the straight line trajectory $\mathbf{R}(t)=(b,0,v_Pt)$ with impact parameter b and constant velocity v_P. The mean-field potential $v_{ee}(\mathbf{r},t)$ accounts for the electron-electron interaction in an effective manner, and in general depends on time. We note that the time-dependent density functional theory ensures the existence of a multiplicative operator v_{ee} that includes all electron-electron interaction effects exactly [12]. In practice, approximations have to be introduced, as the functional form of the exact potential is not known.

We decompose v_{ee} into a contribution, which describes the electron-electron interaction in the undisturbed atomic target ground state before the collision and a contribution, which accounts for the variation of v_{ee} due to the response of the electronic system in the presence of the projectile

$$v_{ee}(\mathbf{r},t)=v_{ee}^0(r)+\delta v_{ee}(\mathbf{r},t). \tag{3}$$

As a particular model for the undisturbed atomic potential $v_{ee}^0(r)$ we choose the exchange-only version of the optimized potential method (OPM) [8]. In this model, self-interaction contributions contained in the Hartree energy are cancelled exactly and the correct asymptotic behavior

$$v_{ee}^0(r)=v_{ee}^{\mathrm{OPM}}(r)\overset{r\to\infty}{\to}\frac{N-1}{r} \tag{4}$$

is ensured. The exact treatment of exchange effects in the OPM was found to be important for collision calculations [4,5]. The no-response approximation of our previous work corresponds to the assumption

$$\delta v_{ee}(\mathbf{r},t)=0. \tag{5}$$

This approximation is justified for fast collisions, for which the spatial electronic distribution does not change considerably during the interaction time. Furthermore, we showed that it yields reliable results for one-electron transitions, such as single capture and single ionization down into the tens of keV/amu range, whereas we found evidence that for a satisfactory description of multiple-electron processes the inclusion of time-dependent screening effects is required [6,7].

As mentioned in the Introduction, the implementation of microscopic models for δv_{ee} is very demanding. In order to assess the influence of time-dependent screening effects without increasing the computational costs significantly we propose a simple model, which is similar to the one we used in a recent study of p^-+Ne collisions [6]. The model is designed to account in a global fashion for the increasing attraction of the target potential as ionization and electron capture set in during the collision. We define

$$v_{\mathrm{eff}}^T(\mathbf{r},t)=-\frac{Q_T}{r}+v_{ee}(\mathbf{r},t) \tag{6}$$

and assume that v_{eff}^T can be approximated by a linear combination of ionic ground-state potentials $v_q(r)$ weighted with the time-dependent probabilities $P_q^{\mathrm{loss}}(t)$ to create the corresponding charge states in the collision

$$v_{\mathrm{eff}}^T(\mathbf{r},t)\approx v_{\mathrm{eff}}^T(r,t)=\sum_{q=0}^{N}P_q^{\mathrm{loss}}(t)v_q(r). \tag{7}$$

Furthermore, we assume that the $v_q(r)$ can be expressed by the self-consistent scaled potential of the neutral target atom for all charge states q in the following way. We write the static atomic potential as

$$v_0(r)=-\frac{Q_T}{r}+v_{ee}^0(r) \tag{8}$$

and define

$$v_q(r)=\begin{cases} v_0(r) & \text{for}\quad q=0 \\ v_0(r)-\dfrac{q-1}{N-1}v_{ee}^0(r) & \text{for}\quad q\geqslant 1. \end{cases} \tag{9}$$

Equation (9) is best understood by considering some limiting cases, which are easily deduced from the asymptotic behav-

ior of $v_{ee}^0(r)$ [Eq. (4)] and the charge balance $Q_T=N$ for a neutral target atom: (1) for $q=N$, $v_q(r)$ reduces to the bare Coulomb potential of the target nucleus, i.e., $-Q_T/r$; (2) for $q=0$, $v_q(r)$ equals the OPM potential of the neutral atom; (3) for $q=1$, $v_q(r)$ is also chosen to be equal to the neutral atom case; (4) for $q>1$, $v_q(r)$ has an asymptotic behavior of type $-q/r$.

To explain the choice of potentials in Eq. (9) and in particular the identical choice for $q=0$ and $q=1$ we provide the following remarks. The potentials defined in Eq. (9) are used to form the mean-field potential (7) which is employed in the time propagation of the orbitals. A TDHF-like mean-field potential has the property that dynamical screening sets in immediately when a small fractional amount of charge has been removed from the target. This effect is caused by the statistical nature of the TDHF approximation whereby all channels are described by a single mean field. It is considered undesirable when one is interested primarily in single ionization or capture. To overcome the associated problems in photoionization a ''frozen TDHF'' approximation was introduced [26]. Our choice of a common potential for $q=0,1$ in the superposition (7) attempts to correct the problem within the TDHF mean field for the collisional kinematic ranges where zerofold to onefold electron removal dominates.

Similarly to Eqs. (7), (8), and (9) one can incorporate a time-dependent screening potential on the projectile center in the description in order to account for the reduced attraction to the projectile as electrons are captured during the collision. This effect is neglected in the present study. It is evident that it will be particularly important for highly charged ion impact at low and intermediate energies, for which multiple capture is likely to occur. Furthermore, we note that the interaction between electrons in the continuum is omitted in our model. This is expected to cause no significant errors as long as one is interested in total ionization yields only.

Insertion of Eq. (9) in Eq. (7) yields

$$v_{\mathrm{eff}}^T(r,t)=v_0(r)+\delta v_{ee}(r,t), \tag{10}$$

with

$$\delta v_{ee}(r,t)=\frac{-1}{N-1}\sum_{q=1}^{N}(q-1)P_q^{\mathrm{loss}}(t)v_{ee}^0(r). \tag{11}$$

Using the normalization

$$P_0^{\mathrm{loss}}(t)=1-\sum_{q=1}^{N}P_q^{\mathrm{loss}}(t) \tag{12}$$

and the definition of the net electron loss as the average number of removed electrons

$$P_{\mathrm{net}}^{\mathrm{loss}}(t)=\sum_{q=1}^{N}qP_q^{\mathrm{loss}}(t) \tag{13}$$

the response potential [Eq. (11)] can be cast into the form

$$\delta v_{ee}(r,t)=-\frac{Q_s(t)}{N-1}v_{ee}^0(r), \tag{14}$$

with the screening function $Q_s(t)$

$$Q_s(t)=P_{\mathrm{net}}^{\mathrm{loss}}(t)+P_0^{\mathrm{loss}}(t)-1. \tag{15}$$

To make use of this ansatz we need explicit expressions for the time-dependent quantities $P_{\mathrm{net}}^{\mathrm{loss}}$ and P_0^{loss}. As in our previous work [5,7] we rely on a channel representation of the single-particle solutions $\psi_i(t)$ and calculate the net electron loss according to

$$P_{\mathrm{net}}^{\mathrm{loss}}(t)=N-\sum_{i=1}^{N}\sum_{v=1}^{V}|\langle\varphi_v|\psi_i(t)\rangle|^2, \tag{16}$$

where the (finite) set $\{|\varphi_v\rangle, v=1,\ldots,V\}$ contains all bound target states populated noticeably in the collision process. With the interpretation of $P_{\mathrm{net}}^{\mathrm{loss}}/N$ as the average single-particle probability for electron loss from the target we obtain the probability P_0^{loss} from the binomial formula

$$P_0^{\mathrm{loss}}(t)=\left(1-\frac{P_{\mathrm{net}}^{\mathrm{loss}}(t)}{N}\right)^N. \tag{17}$$

The remaining question of how to choose the channel functions $|\varphi_v\rangle$ is connected to the projection problem mentioned in the Introduction. In order to ensure a meaningful analysis of the single-particle solutions $\psi_i(t)$, the transition amplitudes

$$c_v^i(t)=\langle\varphi_v|\psi_i(t)\rangle \tag{18}$$

have to become stable after the collision process ($t\to\infty$) up to an oscillatory energy phase. This boundary condition of the scattering problem is fulfilled, when the channel functions obey the time-dependent single-particle Schrödinger equation (1) for asymptotic times

$$[\hat{h}(t)-i\partial_t]|\varphi_v\rangle|_{t\to\infty}=0. \tag{19}$$

With this requirement one obtains for the time derivative of the amplitudes (18)

$$\begin{aligned}\dot{c}_v^i|_{t\to\infty}&=\partial_t\langle\varphi_v|\psi_i(t)\rangle|_{t\to\infty}\\&=-i\langle[\hat{h}(t)-i\partial_t]\varphi_v|\psi_i(t)\rangle|_{t\to\infty}=0,\end{aligned} \tag{20}$$

where we have used Eq. (1). In the no-response approximation Eq. (19) is fulfilled by the eigenfunctions of the undisturbed target atom, if one disregards the long-range Coulomb interaction with the projectile. Although not correct formally, this approximation can be justified from a practical point of view, when the single-particle equations are propagated so far that the projectile does not cause channel couplings in the target. Similarly, eigenfunctions of the moving projectile subsystem are the appropriate channel functions for the analysis of electron capture processes. However, if a time-dependent screening potential is included in the single-particle Hamiltonian [Eq. (2)] the channel functions of the

undisturbed target and projectile subsystems lead generally to fluctuating transition probabilities. This has been observed in several TDHF calculations [16,20].

Let us exemplify this point for our specific model [Eq. (14)]. We assume that the solutions of the single-particle equations (1) can be expanded according to

$$|\psi_i(t)\rangle = \sum_{v=1}^{\infty} c_v^i(t)|\varphi_v\rangle, \tag{21}$$

where the $|\varphi_v\rangle$ are bound target states for $v=1,\ldots,V$, travelling bound projectile states for $v=V+1,\ldots,V+K$, and discrete states, which represent the continuum for $v>V+K$. For asymptotic internuclear separations the states can be assumed to be orthonormal. If we use stationary target orbitals $|\varphi_v^0\rangle$ in the analysis

$$|\varphi_v\rangle \equiv |\varphi_v^0\rangle, \quad v=1,\ldots,V, \tag{22}$$

which fulfill the eigenvalue equation

$$\left(-\frac{1}{2}\Delta + v_0(r)\right)|\varphi_v^0\rangle = \varepsilon_v^0|\varphi_v^0\rangle \tag{23}$$

we obtain for the time-derivative of the transition amplitudes to bound target states [cf. Eq. (20)]

$$\begin{aligned}
\dot{c}_v^i|_{t\to\infty} &= -i\langle\varphi_v^0|\hat{h}(t)|\psi_i(t)\rangle|_{t\to\infty} \\
&= -i\left(\varepsilon_v^0 c_v^i(t) + \sum_{v'=1}^{\infty}\langle\varphi_v^0|\delta v_{ee}(t)|\varphi_{v'}\rangle c_{v'}^i(t)\right)_{t\to\infty} \\
&= -i\left(\varepsilon_v^0 c_v^i(t) - \frac{Q_s(t)}{N-1}\right. \\
&\quad \left.\times\sum_{v'=1}^{\infty}\langle\varphi_v^0|v_{ee}^0|\varphi_{v'}\rangle c_{v'}^i(t)\right)_{t\to\infty}, \\
&\qquad v=1,\ldots,V.
\end{aligned} \tag{24}$$

The response potential couples all states, and thus leads to fluctuating transition probabilities. The fluctuations may persist for all times, since no general argument can be found for the asymptotic decrease of the coupling matrix elements. Only the coupling between bound target and projectile states will fade out because of the vanishing overlap between these states for $R\to\infty$. For the same reason, transition probabilities for electron capture, calculated by projection onto undisturbed moving projectile states, are not affected by our specific target-centered response potential and become stable.

Similarly to Eq. (24) we obtain for the time derivative of the net electron loss $P_{\text{net}}^{\text{loss}}$ [Eq. (16)]

$$\begin{aligned}
\dot{P}_{\text{net}}^{\text{loss}}|_{t\to\infty} &= 2\frac{Q_s(t)}{N-1}\sum_{i=1}^{N}\sum_{v=1}^{V}\sum_{v'>V+K}^{\infty}\langle\varphi_v^0|v_{ee}^0|\varphi_{v'}\rangle \\
&\quad\times \mathrm{Im}[c_v^{i\,*}(t)c_{v'}^i(t)]|_{t\to\infty},
\end{aligned} \tag{25}$$

where we have used

$$\langle\varphi_v^0|v_{ee}^0|\varphi_{v'}\rangle = \langle\varphi_{v'}|v_{ee}^0|\varphi_v^0\rangle, \tag{26}$$

as well as the fact that all terms with $v'\leqslant V$ cancel, and the overlaps between bound target and projectile states vanish asymptotically. The net electron loss fluctuates for all times as the undisturbed atomic target functions $|\varphi_v^0\rangle$ are coupled to the continuum states via the response potential.

For our specific model, where the time-dependence of the response potential is driven by the net electron loss, a solution of the problem of fluctuating transition probabilities can be found. To this end, the analysis at the target center and the definition of the net electron loss have to be based on eigenfunctions $|\varphi_v(t)\rangle$ of the Hamiltonian that includes the response potential

$$|\varphi_v\rangle \equiv |\varphi_v(t)\rangle, \quad v=1,\ldots,\tilde{V}, \tag{27}$$

$$\left(-\frac{1}{2}\Delta + v_0(r) + \delta v_{ee}(r,t)\right)|\varphi_v(t)\rangle = \varepsilon_v(t)|\varphi_v(t)\rangle \tag{28}$$

in contrast to the eigenstates $|\varphi_v^0\rangle$ of the undisturbed target atom, which satisfy Eq. (23). Equation (28) represents an eigenvalue problem, in which the time t appears as a parameter. In analogy to Eq. (16) we assume that the finite set $\{|\varphi_v(t)\rangle, v=1,\ldots,\tilde{V}\}$ is suitable to describe the total population of bound target states in the collision. In the Appendix, we show that all transition probabilities become stable for $t\to\infty$ in this case. From a physical point of view it appears quite natural to use the eigenfunctions $|\varphi_v(t)\rangle$ of Eq. (28) for the analysis, as they are consistent with the time-dependent mean-field description and correspond to the average fractional charge state on the target atom after the collision. Note that they depend on time parametrically, since the response potential itself depends on time via the net electron loss [cf. Eq. (14)], or the solutions of Eq. (1) in more general cases for δv_{ee}. In these more general situations the asymptotic stability of the transition probabilities cannot be ensured, because the eigenfunctions $|\varphi_v(t)\rangle$ do not obey the boundary condition (19). This is evident from Eq. (A6) of the Appendix. Therefore, our analysis does not solve the TDHF projection problem in general. Nevertheless, it allows us to extract well-defined transition probabilities for our specific model. It may also serve as a starting point for the analysis of calculations with microscopic response potentials δv_{ee}, as the present discussion can be carried over to the monopole contribution in the mean-field potential in the general TDHF case.

III. COMPUTATIONAL ASPECTS

As the methods for the solution of the time-dependent single-particle equations (1) and the extraction of transition probabilities for net and multiple ionization and capture events are similar to the ones we used in our previous work [5,7,9], we give only a short summary in this section. The basis generator method (BGM) is used to propagate the

single-particle equations (1) with the response potential (14); i.e., the orbitals $\psi_i(t)$ are expanded in terms of dynamically adapted basis states

$$|\psi_i(t)\rangle = \sum_{\mu=0}^{M} \sum_{v=1}^{V} d^{i}_{\mu v}(t) |\chi^{\mu}_{v}(t)\rangle, \tag{29}$$

$$|\chi^{\mu}_{v}(t)\rangle = [W_P(t)]^{\mu} |\varphi^{0}_{v}\rangle, \quad \mu = 0, \ldots, M, \tag{30}$$

where W_P denotes the suitably regularized projectile potential. In the present calculation we have included all undisturbed target states $|\varphi^0_v\rangle$ of the *KLMN* shells calculated numerically on a fine mesh and 100 functions from the set $\{|\chi^{\mu}_{v}(t)\rangle, \mu \geqslant 1\}$ up to order $\mu = 8$ in the basis.

Our choice of the response potential [Eq. (14)] requires to calculate the net electron loss $P^{\rm loss}_{\rm net}$ [Eq. (16)] in each time step. In order to ensure the asymptotic stability of all transition probabilities the calculation of $P^{\rm loss}_{\rm net}$ has to rely on the states $|\varphi_v(t)\rangle$ [Eq. (28)]. We diagonalize the Hamiltonian of Eq. (28) in the BGM basis to obtain (real) coefficients $a^{v}_{\mu' v'}(t)$

$$|\varphi_v(t)\rangle = \sum_{\mu'=0}^{M} \sum_{v'=1}^{V} a^{v}_{\mu' v'}(t) |\chi^{\mu'}_{v'}(t)\rangle, \tag{31}$$

and find for the net electron loss

$$P^{\rm loss}_{\rm net}(t) = N - \sum_{i=1}^{N} \sum_{v=1}^{\tilde{V}} \sum_{\mu'\mu''=0}^{M} \sum_{v'v''=1}^{V} a^{v}_{\mu' v'}(t) \times a^{v}_{\mu'' v''}(t)\, d^{i}_{\mu' v'}(t)\, d^{i\,*}_{\mu'' v''}(t), \tag{32}$$

with the expansion coefficients $d^{i}_{\mu' v'}(t)$ of Eq. (29). Note that due to the finiteness of the BGM basis only a limited number of states $|\varphi_v(t)\rangle$ can be represented with reasonable accuracy. We have compared energy eigenvalues obtained from the diagonalization in the BGM basis with ''exact'' eigenvalues obtained from a numerical solution of the stationary Schrödinger equation (28) for a few arbitrary choices of $P^{\rm loss}_{\rm net}$ in the response potential. Furthermore, we have studied transition probabilities to numerically calculated states $|\varphi_v(t)\rangle$, and to states represented in the BGM basis via Eq. (31). These tests indicated that a proper choice of $\tilde{V}$ in Eq. (32) is given by $\tilde{V} = V$, i.e., the populations of all states in the *KLMN* shells of the fractionally ionized target system are added in order to calculate the net electron loss in each time step of the propagation.

At the final time $t = t_f$, we calculate the net electron capture $P^{\rm cap}_{\rm net}$ by explicit projection of the single-particle solutions onto traveling He^+ states $|\varphi^P_k\rangle$

$$P^{\rm cap}_{\rm net}(t_f) = \sum_{i=1}^{N} \sum_{k=1}^{K} |\langle \varphi^{P}_{k}(t_f) | \psi_i(t_f)\rangle|^2. \tag{33}$$

K is chosen to include all projectile states of the *KLM* shells. Assuming that the summations in $P^{\rm loss}_{\rm net}$ and $P^{\rm cap}_{\rm net}$ are sufficient to cover the bound parts of the electronic density we can define the net ionization $P^{\rm ion}_{\rm net}$ by

$$P^{\rm ion}_{\rm net}(t_f) = P^{\rm loss}_{\rm net}(t_f) - P^{\rm cap}_{\rm net}(t_f). \tag{34}$$

The more detailed calculation of capture and ionization events associated with specific final charge states of the projectile and target ions is based on the shell-specific trinomial analysis [27] and the analysis in terms of products of binomials that we have introduced in Ref. [7]. Whereas one obtains nonzero transition probabilities for unphysical higher-order capture processes in the trinomial analysis (i.e., capture of more than two electrons in the present case of He^{2+} projectiles), these transitions are avoided in the analysis in terms of products of binomials. In this model the net electron capture (33) is distributed over the physical capture channels, i.e., over single and double capture in the present case, by carrying out binomial statistics with the new single-particle probability $P^{\rm cap}_{\rm net}/2$. This *k*-fold capture probability is multiplied by an independent *l*-fold binomial ionization probability to obtain P_{kl}, the probability for *k*-fold capture accompanied by *l*-fold ionization. Obviously, the model is only well-defined as long as $P^{\rm cap}_{\rm net} \leqslant 2$. If $P^{\rm cap}_{\rm net}$ exceeds this value, negative probabilities for specific multiple-electron transitions arise. This has to be avoided by capping the net capture probabilities in these situations.

Finally, we note that we have also calculated multiple-electron transition events for some test cases on the basis of the formalism of inclusive probabilities [28], which accounts for the Pauli blocking in the final states. However, we have not found substantially different results when comparing to the trinomial analysis. In particular, the unphysical triple capture is not considerably suppressed, as transition amplitudes to several individual projectile states, whose combination is not forbidden by the Pauli principle, are found to contribute.

IV. RESULTS

A. Net electron loss, ionization, and capture

Before we compare our results for net electron loss, ionization, and capture cross sections in $He^{2+} + Ne$ collisions with experimental data we illustrate the asymptotic stability of transition probabilities, and discuss the influence of the time-dependent screening potential on the net probabilities in a global fashion.

In Fig. 1 we show the net electron loss $P^{\rm loss}_{\rm net}$ as a function of the internuclear separation for the specific situation of projectile energy $E_P = 100$ keV/amu and impact parameter $b = 1$ a.u. The results of three different calculations are included in the figure: (1) the present model for time-dependent screening according to Eqs. (14)–(17) and (32); (2) a calculation that also relies on Eqs. (14)–(17), but in which the net electron loss is defined with respect to the undisturbed atomic target states $|\varphi^0_v\rangle$ that obey Eq. (23); (3) a calculation in the no-response approximation [Eq. (5)]. We note that we have used the same BGM basis set in all calculations.

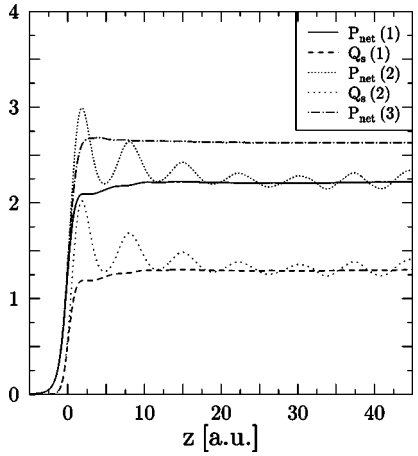

FIG. 1. Net electron loss probability $P_{\mathrm{net}}^{\mathrm{loss}}$ (16) and screening function Q_s (15) as a function of the internuclear separation $z = v_P t$ for $He^{2+} + Ne$ collisions. The different calculations (1)–(3) are explained in the text.

In agreement with our theoretical analysis the time-dependent screening calculation based on the states $|\varphi_v(t)\rangle$ yields stable results, whereas $P_{\mathrm{net}}^{\mathrm{loss}}$ oscillates, when calculated with respect to the states $|\varphi_v^0\rangle$. The oscillatory behavior illustrates the lack of synchronization between the time-dependent potential and the undisturbed target states $|\varphi_v^0\rangle$. Around the closest approach ($z=0$ a.u.), the projectile potential reduces the population of the bound states $|\varphi_v^0\rangle$, which, in turn, feeds the response potential and increases the attraction of the target, so that a certain amount of probability is recaptured to the bound states. This interplay can only be balanced, when the functions $|\varphi_v(t)\rangle$ are used, which account for the response potential.

We note that the average value of the oscillating curve coincides quite well with the stable result of calculation (1) at large distances. Compared to the no-response calculation $P_{\mathrm{net}}^{\mathrm{loss}}$ is reduced by approximately 15% for the specific impact parameter and energy. In addition to $P_{\mathrm{net}}^{\mathrm{loss}}$ we have included the function Q_s [Eq. (15)] in Fig. 1, which governs the response potential (14). As a matter of course Q_s shows the stable or oscillating behavior of the corresponding net electron loss. Around the closest approach one observes a delayed rise when comparing to $P_{\mathrm{net}}^{\mathrm{loss}}$. This is a desired consequence of the particular choice of potentials in Eq. (9) that has been discussed in Sec. II. As long as the average number of removed electrons is smaller than or comparable to one, the magnitude of the response potential δv_{ee} remains small. This is in contrast to an alternative screening model, in which δv_{ee} is driven directly by $P_{\mathrm{net}}^{\mathrm{loss}}$ [6]. When $P_{\mathrm{net}}^{\mathrm{loss}}$ becomes considerably larger than one, the elastic probability P_0^{loss} approaches zero [see Eq. (17) and note that $N=10$], and thus the screening function Q_s approaches $P_{\mathrm{net}}^{\mathrm{loss}} - 1$.

We have checked that for neither of the screening models does the net electron capture $P_{\mathrm{net}}^{\mathrm{cap}}$ ever exhibit oscillatory behavior. As our specific response potential (14) is centered around the target nucleus the asymptotic Schrödinger equation in the projectile system [see Eq. (19)] is fulfilled by traveling hydrogenic eigenstates for the nuclear charge $Q_P = 2$, which we use to calculate $P_{\mathrm{net}}^{\mathrm{cap}}$ from the propagated orbitals. Fluctuations similar to the ones shown in Fig. 1 are expected when a response potential at the projectile center would be included in the calculation.

In Figs. 2 and 3 we show the net ionization $P_{\mathrm{net}}^{\mathrm{ion}}$ and the net capture $P_{\mathrm{net}}^{\mathrm{cap}}$ after the collision ($z_f = 45$ a.u.) as functions of impact parameter b and impact energy E_P to provide a general picture of the collision system and to demonstrate the role of time-dependent screening. In what follows, we solely employ the screening model that relies on the states $|\varphi_v(t)\rangle$, and which gives stable results, i.e., Eqs. (14)–(17) and (32) are used. The net ionization $P_{\mathrm{net}}^{\mathrm{ion}}$ has a relatively simple structure (Fig. 2). It is largest at impact energies 100 keV/amu $\leqslant E_P \leqslant$ 200 keV/amu and at small impact parameters b. Furthermore, $P_{\mathrm{net}}^{\mathrm{ion}}$ is confined to rather close collisions at low energies, but extends towards larger values of b at higher

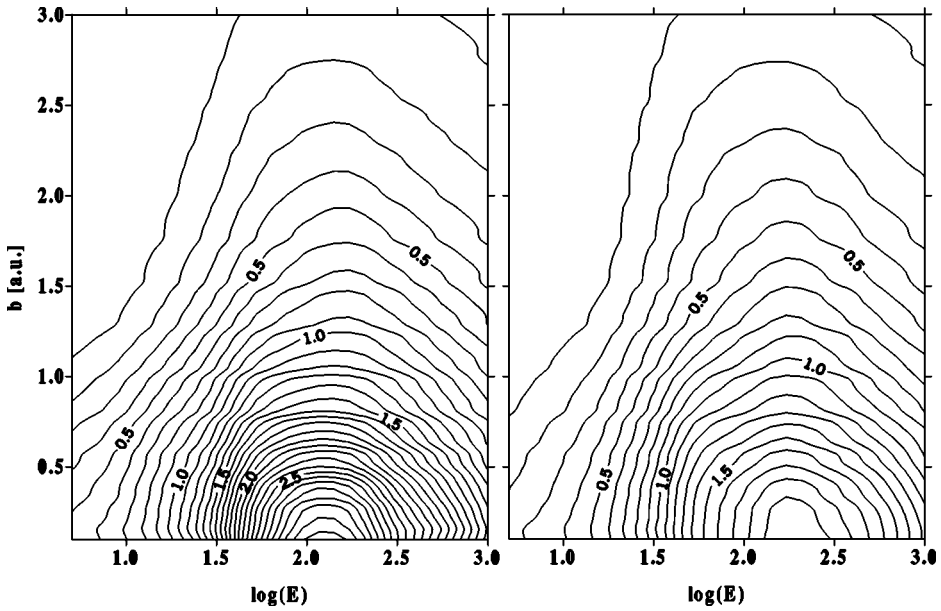

FIG. 2. Net ionization probability $P_{\mathrm{net}}^{\mathrm{ion}}$ as a function of the logarithm ($\log_{10}$) of the impact energy E_P (in keV/amu) and the impact parameter b (in a.u.) for $He^{2+} + Ne$ collisions. Left panel: calculation in the no-response approximation; right panel: calculation including time-dependent screening according to Eqs. (14)–(17), and (32).

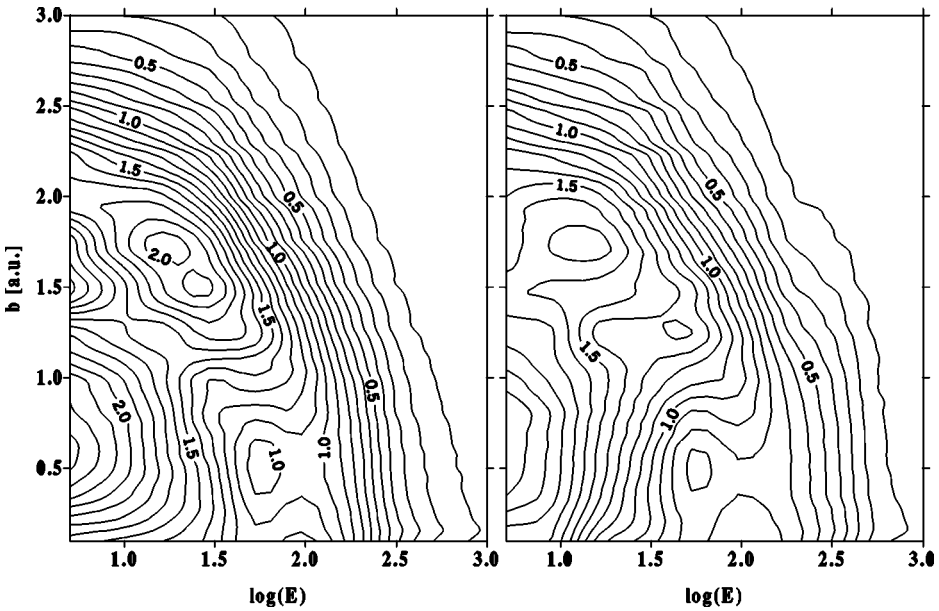

FIG. 3. Net electron capture probability $P_{\mathrm{net}}^{\mathrm{cap}}$ as a function of the logarithm ($\log_{10}$) of the impact energy E_P (in keV/amu) and the impact parameter b (in a.u.) for $He^{2+}+Ne$ collisions. Left panel: calculation in the no-response approximation; right panel: calculation including time-dependent screening according to Eqs. (14)–(17), and (32).

E_P. The inclusion of time-dependent screening effects does not change these general trends, but smoothly depletes $P_{\mathrm{net}}^{\mathrm{ion}}$ except for large b and high E_P. The maximum value (reached at the smallest impact parameter in our calculation, $b=0.1$ a.u.) is reduced from approximately 3.4 to 1.9 and is shifted slightly to higher E_P.

The general reduction of $P_{\mathrm{net}}^{\mathrm{ion}}$ can be easily understood from the increased attraction of the target when time-dependent screening is included. This is also reflected in the energy eigenvalues of the orbitals, which are to be interpreted as average ionization potentials within the time-dependent mean-field approximation. For the $2p$ electrons, which are dominantly ionized, the eigenvalue changes from $\varepsilon_{\mathrm{Ne}(2p)}=-0.85$ a.u. for the neutral system to $\varepsilon_{\mathrm{Ne}(2p)}(t_f)=-2.98$ a.u for the corresponding eigenstate $|\varphi_v(t_f)\rangle$ of Eq. (28) at $b=0.1$ a.u. and $E_P=150$ keV/amu.

The shape of the net electron capture probability $P_{\mathrm{net}}^{\mathrm{cap}}$ as a function of b and E_P is more involved (Fig. 3). For both calculations, with and without the inclusion of time-dependent screening, two regions can be observed, where $P_{\mathrm{net}}^{\mathrm{cap}}$ exhibits pronounced local maxima. The largest values are reached at the lowest impact energy in our calculation ($E_P=5$ keV/amu) in the impact parameter range 0.5 a.u. $\leqslant b \leqslant 1$ a.u., while the second maximum is located at around $b\approx 1.75$ a.u. and at slightly higher E_P. Compared to the net ionization (Fig. 2), $P_{\mathrm{net}}^{\mathrm{cap}}$ is confined to rather small impact energies, but extends to larger impact parameters. In general, the time-dependent screening reduces $P_{\mathrm{net}}^{\mathrm{cap}}$, but small regions are found where the effect is reversed. This uneven behavior can be understood from the changing energy differences between the initial target and final projectile states, when the response potential is included in the calculation. In the no-response approximation the dominant capture process at low E_P is the transfer of electrons from the initial $2s$ orbital ($\varepsilon_{\mathrm{Ne}(2s)}=-1.72$ a.u.) to the ground state of the projectile [5]. The inclusion of time-dependent screening lowers the energy eigenvalues of the target states and diminishes the capture of $2s$ electrons as their energy difference to the projectile ground state ($\varepsilon_{\mathrm{He}}^{+(1s)}=-2$ a.u.) increases in the important kinematic regions. By contrast, the orbital energies of the $2p$ electrons approach or even cross the value of -2 a.u. during the collision, and are thus more likely to be captured when the response potential is included. Evidently, the situation might change again when time-dependent screening of the projectile nucleus would also be taken into account.

The total cross sections (TCS) for net electron loss, ionization, and capture are displayed in Figs. 4, 5, and 6 in comparison with experimental data of Refs. [22,23]. For the calculation with the response potential (14) our results agree very well with the measurements at impact energies $E_P \geqslant 20$ keV/amu, whereas the TCS in the no-response approximation are in general higher and lie outside the experimental error bars.

At high energies the results of both sets of calculations merge. This behavior, which is also seen on a more differential level in Figs. 2 and 3 confirms our earlier assumption that time-dependent screening is not effective in collisions,

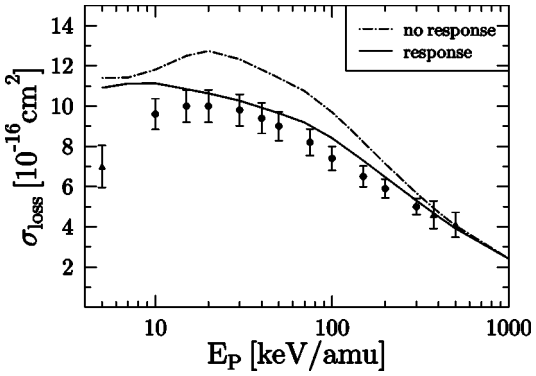

FIG. 4. Total cross section for net electron loss as a function of impact energy for $He^{2+}+Ne$ collisions. Theory: present calculations with and without inclusion of time-dependent screening denoted by the full curve and chain curve, respectively. Experiment: closed circles [22]; closed triangles [23] obtained by extrapolating the data of Ref. [22].

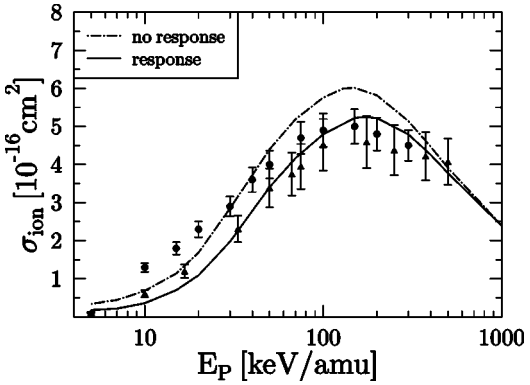

FIG. 5. Total cross section for net ionization as a function of impact energy for $He^{2+}+Ne$ collisions. Theory: present calculations with and without inclusion of time-dependent screening denoted by the full curve and chain curve, respectively. Experiment: closed circles [22]; closed triangles [23].

where the projectile moves considerably faster than the outershell target electrons. The electrons are hit suddenly, and do not react to the changing mean-field attraction of the target. We note that this is not a trivial consequence of the small magnitude of the response potential (14) in this region. In fact, we have found very similar results with the alternative model of Ref. [6], where time-dependent screening is driven directly by $P_{\rm net}^{\rm loss}$ and and sets in in the $0<\bar{q}\leqslant 1$ range in contrast to our present choice of Eqs. (7) and (9). However, these calculations resulted in considerably smaller TCS at intermediate impact energies when compared to the present model and the experimental data. In this region, the present time-dependent screening model reduces the no-response TCS by the appropriate amount to approach the experimental values. For the ionization channel the agreement with the data of Ref. [23] is very good down to the lowest impact energies. We note that the author of Ref. [23] argues that his results are more accurate than the earlier measurements of Ref. [22].

For the capture channel, however, we find discrepancies with both experimental data sets for $E_P\leqslant 20$ keV/amu and a

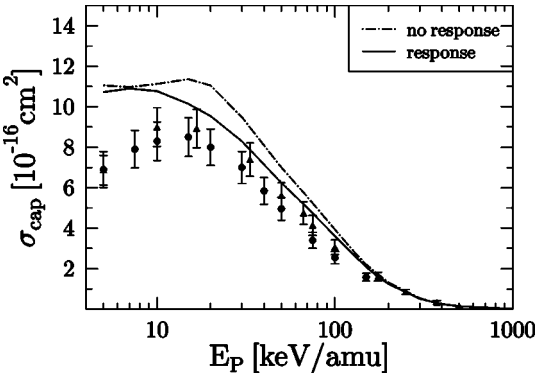

FIG. 6. Total cross section for net electron capture as a function of impact energy for $He^{2+}+Ne$ collisions. Theory: present calculations with and without inclusion of time-dependent screening denoted by the full curve and chain curve, respectively. Experiment: closed circles [22]; closed triangles [23].

different trend towards even lower energies. Around 10 keV/amu the influence of the response potential on the TCS is rather small. As has been discussed above, this is partly due to a compensation of the behavior of electrons of different initial subshells. As electron capture at low impact energies is sensitive to the strength of intermediate couplings, it is evident that the specific form of the response potential is probed by this process. Obviously, our present (spherical) model is too crude to yield accurate results in this region. We have performed some test calculations, where a spherical model for the time-dependent screening of the projectile nucleus was included, but the results did not improve considerably upon the data shown in Fig. 6. It is of interest to investigate, if the disagreement with the experimental data at low energies can be resolved when a microscopic model for time-dependent screening, e.g., the extension of the OPM to the time-dependent case [29], would be considered. For the $He^{2+}+He$ collision system full TDHF calculations indicated that an accurate description of capture at low projectile energies requires to go beyond the IPM in order to account for correlation effects [13,15]. We note, however, that this conclusion was drawn with respect to the individual description of the single and double capture channels. For the more global net capture TCS the situation is not that obvious. In our opinion the published $He^{2+}+He$ data do not provide clear evidence for a failure of TDHF to predict net capture down to projectile energies at around 5 keV/amu.

B. Multiple electron loss, ionization, and capture

The quality of the present calculations and the effects of time-dependent screening are investigated further in this section by analyzing the final charge-state distributions of projectile and target. As described in Sec. III cross sections σ_{kl} for k-fold capture with simultaneous l-fold ionization are calculated from the single-particle solutions by using the trinomial and the products of binomials analyses [7]. The more inclusive TCS for q-fold electron loss from the target σ_q are obtained from σ_{kl} by

$$\sigma_q=\sum_{kl,k+l=q}\sigma_{kl}\,. \tag{35}$$

We note that the summation of the trinomial data gives cross sections, which can also be calculated directly by using the binomial analysis for q-fold electron loss from the target [5]. Corresponding results are shown in Fig. 7 along with experimental data. The measurements for σ_{kl} of Ref. [23] have been added according to Eq. (35), while we have normalized the *relative* cross sections for $q=2,3$ of Ref. [24] to our present results for onefold electron loss (σ_1).

For $q=1$ our results are in very good agreement with the experimental data over the entire energy range. The curve is rather flat, i.e., the energy dependence of onefold electron loss is weak. As expected and desired, the effects of the time-dependent screening are small for this channel. For most impact energies the cross sections are slightly increased by their inclusion, although the net electron loss is reduced (see Fig. 4). This is a consequence of the statistical analysis,

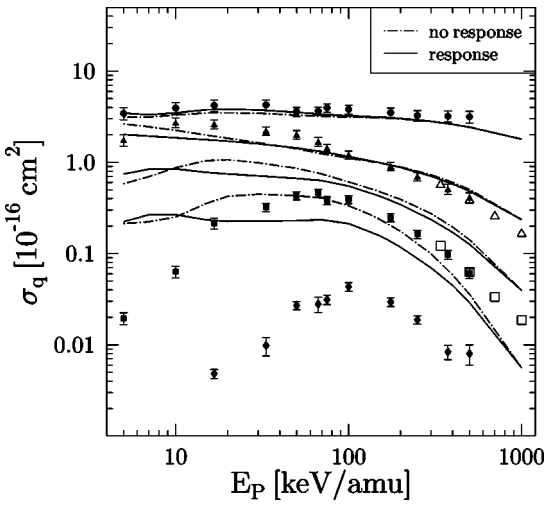

FIG. 7. Total cross sections for q-fold electron loss ($q=1\cdots4$) as a function of impact energy for $He^{2+}+Ne$ collisions. Theory: present calculations with and without inclusion of time-dependent screening (denoted by the full curves and chain curves, respectively) according to the standard binomial analysis. Experiment: closed symbols [23]; open symbols [24] normalized to the theoretical cross sections for onefold electron loss. The error bars are smaller than the size of the symbols.

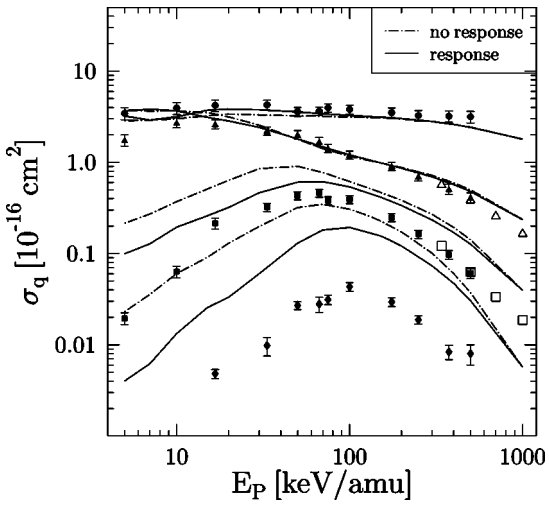

FIG. 8. Total cross sections for q-fold electron loss ($q=1\cdots4$) as a function of impact energy for $He^{2+}+Ne$ collisions. Theory: present calculations with and without inclusion of time-dependent screening (denoted by the full curves and chain curves, respectively) according to the analysis in terms of products of binomials. Experiment: same as in Fig. 7.

in which a decrease in the shell-specific single-particle probabilities can lead to an increase in the multiple-electron transition probabilities for low multiplicities.

For $q=2$ the effects of time-dependent screening are also rather small. Only at low impact energies is the cross section reduced noticeably. The experimental data lie above our results in this region except for the data point at $E_P=5$ keV/amu. Good agreement is found for higher energies up to $E_P\leqslant500$ keV/amu, whereas the experimental cross sections are smaller than our results for even faster collisions. This discrepancy is more pronounced for σ_3 and σ_4, and is hardly affected by time-dependent screening. At intermediate impact energies σ_3 and σ_4 are considerably reduced by the inclusion of the response potential (14), but the experimental data are still substantially smaller than these results. At present it remains open, whether the discrepancy can be resolved within the IPM by use of a more refinded time-dependent screening model.

At low impact energies, where capture dominates the electron loss from the target, the need for a microscopic screening model has already been discussed in Sec. IV A. Obviously, the deficiencies seen in the net electron capture in this region (Fig. 6) are also mirrored in the multiple-electron cross sections. Our calculations yield large single-particle probabilities for electron capture at low impact energies, which feed the higher charge states when combined in terms of the standard binomial and trinomial analyses. A closer inspection of the data shows that σ_3 and σ_4 are dominated by the unphysical multiple-capture ($k\geqslant3$) channels.

Within the analysis in terms of products of binomials the unphysical $k\geqslant3$ capture is avoided by construction. In fact, σ_3 and σ_4 are considerably reduced in the low to intermediate energy range when using this evaluation method (Fig. 8). They agree in shape with the experimental results, in particular when time-dependent screening is included, but a substantial difference in the absolute magnitude persists for $q\geqslant3$. We note that the improvement in the shape of σ_2 and σ_3 at intermediate energies as compared to the standard binomial analysis (Fig. 7) is remarkable.

The unphysical higher-order capture events are not simply omitted in the products of binomials analysis but redistributed over the physical capture channels. Therefore, an increase of σ_1 and σ_2 at low to intermediate impact energies is observed in Fig. 8. The increase is more pronounced for σ_2 and leads to a crossing of both channels around 10 keV/amu. In this region, we have found that $P_{\rm net}^{\rm cap}$ exceeds the value of two in some impact parameter ranges in the no-response approximation. In these cases we have set $P_{\rm net}^{\rm cap}=2$ in order to avoid negative probabilities for specific multiple-electron transition channels (see Sec. III). When time-dependent screening is included, the calculations yield $P_{\rm net}^{\rm cap}\leqslant2$ with only very few exceptions. Nevertheless, the crossing of σ_1 and σ_2, which is not supported by the experimental data and appears to be artificial, cannot be avoided. Its location clearly indicates, down to which impact energies our calculations give an acceptable description of the collision system. It remains to be seen whether an improved model for time-dependent screening effects can remedy the deficiencies for $E_P\leqslant15$ keV/amu that are observed in the net electron capture (Fig. 6) and the q-fold electron loss with either evaluation method (Figs. 7 and 8).

Finally, we present results for the charge-state correlated cross sections σ_{kl} obtained from the analysis in terms of products of binomials in Fig. 9. A comparison of results obtained from this method with trinomial cross sections was given in Ref. [7] for proton scattering from oxygen atoms

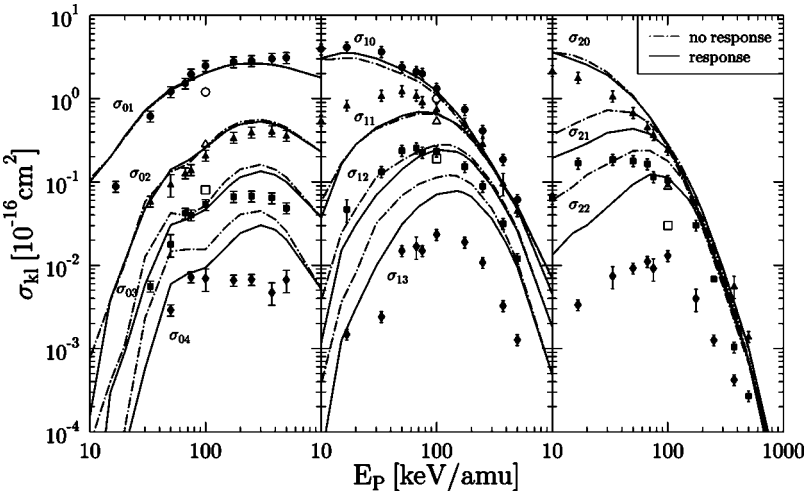

FIG. 9. Total cross sections σ_{kl} for k-fold electron capture with simultaneous l-fold ionization as a function of impact energy for $He^{2+}+Ne$ collisions. Theory: present calculations with and without inclusion of time-dependent screening (denoted by the full curves and chain curves, respectively) according to the analysis in terms of products of binomials; open symbols, calculation included in Ref. [23] for $\sigma_{01}-\sigma_{03}$ (left panel), $\sigma_{10}-\sigma_{12}$ (middle panel), and $\sigma_{20}-\sigma_{21}$ (right panel). Experiment: closed symbols [23].

and will not be repeated here for $He^{2+}+Ne$ collisions. In addition to the experimental results of Ref. [23] we have included values for σ_{kl} in Fig. 9, which were obtained from a pilot calculation in the so-called independent Fermi particle model and were included in Ref. [23]. A preliminary account of the theoretical model used can be found in Ref. [25].

In the left panel of Fig. 9 the pure ionization channels ($k=0$) are shown. For threefold ($l=3$) and fourfold ($l=4$) ionization some structures are observed at intermediate impact energies in the no-response results. These are less pronounced when time-dependent screening is included. The overall agreement of our results for pure ionization with the experimental data is good. Only for impact energies $E_P>200$ keV/amu and $l=3,4$ are our data larger than the measured values indicating that the reduction of the cross sections by the present model for time-dependent screening is not sufficient in this region. For $E_P \geqslant 500$ keV/amu the influence of the response potential δv_{ee} is negligible for all charge states. It is unlikely that a more refined model for δv_{ee} would give substantially different results in this region, where the projectile motion is fast compared to the average velocities of the electrons of the neon $n=2$ shell.

The question arises whether the experimental cross sections at, e.g., 500 keV/amu are in general compatible with the IPM-based analysis. We were able to model single-particle probabilities for ionization (and capture), which generate the experimental cross section distribution at $E_P=500$ keV/amu with reasonable accuracy when combined statistically. The impact-parameter dependences of the fitted single-particle probabilities differ significantly from the results of our BGM calculation. The former are smaller at low b, and extend over a wider range of impact parameters. The BGM results for ionization from the individual neon subshells in turn proved to be in very good agreement with impact-parameter dependent probabilities obtained from the continuum distorted wave with eikonal initial state (CDW-EIS) method [30], which should be reliable at 500 keV/amu [4,5]. Given these findings it is at least doubtful whether the discrepancy with the experimental data can be resolved within the IPM.

The capture channels are displayed in the middle and right panels of Fig. 9. Pure single capture σ_{10} is in good agreement with the experimental data. The inclusion of the response potential δv_{ee} slightly increases the cross section at low projectile energies, while almost no effect is observed for the transfer-ionization channel σ_{11}. Our results are considerably smaller than the experimental values for σ_{11} at impact energies $E_P<100$ keV/amu. Since pure single ionization (σ_{01}) and pure single capture (σ_{10}) are in good agreement with the measurements, the deviations of σ_{11} indicate that this transition cannot be understood as the simple product of the two one-electron processes. Remarkably, the discrepancies with the experimental data are smaller for σ_{12}, whereas our results lie above the measurements for σ_{13} over the entire energy range. The inclusion of time-dependent screening reduces the cross section for low to intermediate energies similar to the case of pure ionization for the same final charge state of the target ($q=4$), but the experimental data are still considerably smaller.

The double capture processes ($k=2$) are only described on a qualitative level by our calculations. We obtain cross sections, which are larger than the experimental values for all degrees of ionization except for two data points at high impact energies. This result reflects the fact that no dynamic screening of the projectile nucleus is included in our present model for δv_{ee}. As a consequence, the analysis of capture events is based on bound He^+ states at the projectile center (see Sec. III), i.e., the electron-electron interaction in the final states is ignored completely in the case of double capture. According to the theoretical analysis of Sec. II the inclusion of a time-dependent screening of the projectile charge would require us to calculate the electron capture with respect to single-particle states, which correspond to the (fractional) final charge state of the projectile and include electron-electron interaction effects in an average manner. It is plausible that this inclusion of screening effects on the projectile will reduce the double-capture channels, while increasing the single-capture contributions in such a way that the agreement with the experimental data will improve for the channels σ_{20}, σ_{21}, and σ_{11} with possibly an overestimation of σ_{10}. However, one has to keep in mind that spherical models for δv_{ee} may be too simple to describe the electronic response in the low to intermediate energy range with reasonable accuracy.

V. CONCLUSIONS

In this paper the role of time-dependent screening in the IPM description of ion-atom collision systems with many active electrons has been investigated. We have proposed a relatively simple model for a potential δv_{ee} that accounts for the response of the electrons in the presence of the projectile, and have addressed the question of how to analyze the solutions of the single-particle equations in order to obtain stable results for all inelastic transitions. The necessary condition for a well-defined analysis is that the single-particle channel functions used to calculate transition probabilities from the propagated orbitals be compatible with the boundary conditions of the collision problem. For the present choice of δv_{ee}, whose time dependence is driven by the net electron loss in a nonlinear way, a suitable set of channel functions $|\varphi_v(t)\rangle$ is given by the eigenstates of the asymptotic single-particle Hamiltonian that includes the (time-dependent) potential δv_{ee}. These states correspond to the average fractional charge state on the target atom after the collision and are consistent with the mean-field description of the process. It remains to be seen whether the ideas of the stability analysis can be extended to situations where δv_{ee} is a more general functional of the time-dependent density.

We have calculated TCS for electron loss, capture, and ionization in $He^{2+}+Ne$ collisions from the solutions of the effective single-particle equations as obtained by use of the basis generator method, while making use of the $|\varphi_v(t)\rangle$ in the probability analysis. We have found that our model for time-dependent screening significantly improves upon results obtained in the no response approximation ($\delta v_{ee}=0$) and yields very good agreement with experimental data in the case of net ionization and net electron capture except at low impact energies. In this region, it is likely that our model of δv_{ee} is too crude, as it does not account for nonspherical response effects and the dynamical screening of the projectile charge.

Very good agreement with experiments has been obtained for the recoil charge state production cross sections σ_q for $q=1,2$ and acceptable agreement for $q=3$ in an energy range from 20 to 1000 keV/amu. This was achieved by two ingredients: the analysis in terms of products of binomials [7] and the time-dependent screening.

The results for charge-state correlated cross sections are also based on the analysis in terms of products of binomials. The time-dependent screening mainly affects multiple particle transitions, while one- and two-electron processes are only slightly modified. This is a desired consequence of the specific model for δv_{ee}, which is designed to suppress response effects in kinematic ranges where zerofold to onefold electron removal dominates. In fact, our results for pure single ionization and pure single capture describe the experimental data very well. The higher-order events are significantly reduced for low to intermediate projectile energies by the inclusion of δv_{ee}, but some serious discrepancies with the experimental results persist. Perhaps the dynamic screening effects have to be turned on more strongly for $q>2$.

At present we can only speculate to which extent these discrepancies might be reduced when a more accurate model for time-dependent screening would be used in the calculations. Further steps into this direction seem feasible and will be the subject of future work. In particular, we would like to point out that the present method to analyze the propagated orbitals with respect to eigenstates of the asymptotic Hamiltonian that includes δv_{ee} may prove to be a solution of the TDHF projection problem from a practical point of view. Ultimately, this analysis along with accurate BGM solutions of the time-dependent single-particle equations including a microscopic response potential may enable us to assess the validity of the IPM and the significance of correlation effects in ion-atom collisions with many active electrons in further detail.

ACKNOWLEDGMENTS

We thank E. Engel for making his OPM atomic structure calculations available to us, and L. Gulyás for the communication of his CDW-EIS results. This work has been supported by the Collaborative Research Grant No. 972997 of the NATO International Scientific Exchange Program, and the Natural Sciences and Engineering Research Council of Canada. One of us (T.K.) gratefully acknowledges financial support of the DAAD.

APPENDIX

In this appendix, we show that all transition probabilities to bound target states become stable for $t\to\infty$, if the analysis and the definition of the net electron loss [Eq. (16)] are based on the states $|\varphi_v(t)\rangle$, which solve the eigenvalue equation (28). Due to Eq. (20) and the asymptotic property

$$\hat{h}(t)|\varphi_v(t)\rangle|_{t\to\infty}=\left(-\frac{1}{2}\Delta+v_0(r)+\delta v_{ee}(r,t)\right)|\varphi_v(t)\rangle|_{t\to\infty}$$
$$=\varepsilon_v(t)|\varphi_v(t)\rangle|_{t\to\infty}, \tag{A1}$$

it is sufficient to demonstrate that

$$\partial_t|\varphi_v(t)\rangle|_{t\to\infty}=0 \tag{A2}$$

for $v=1,\ldots,\tilde{V}$. As a first step we prove

$$\langle\varphi_{v'}(t)|\partial_t|\varphi_v(t)\rangle = \begin{cases} 0 & \text{for} \quad v=v', \\ \dfrac{1}{\varepsilon_v(t)-\varepsilon_{v'}(t)}\langle\varphi_{v'}(t)|\delta\dot{v}_{ee}|\varphi_v(t)\rangle & \text{for} \quad v\neq v'. \end{cases} \tag{A3}$$

For $v\neq v'$ the eigenvalue equation (28) and the orthogonality of the states $|\varphi_v(t)\rangle$ can be used to show

$$[\varepsilon_{v'}(t)-\varepsilon_v(t)]\langle\varphi_{v'}(t)|\partial_t|\varphi_v(t)\rangle$$
$$=\left\langle\varphi_{v'}(t)\left|\left[-\frac{1}{2}\Delta+v_0+\delta v_{ee},\partial_t\right]\right|\varphi_v(t)\right\rangle$$
$$=-\langle\varphi_{v'}(t)|\delta\dot{v}_{ee}|\varphi_v(t)\rangle. \tag{A4}$$

For $v=v'$ one can use the fact that the states $|\varphi_v(t)\rangle$ are normalized for all times. One then finds

$$\langle\varphi_v(t+\Delta t)|\varphi_v(t+\Delta t)\rangle\approx\langle\varphi_v(t)|\varphi_v(t)\rangle+[\langle\partial_t\varphi_v(t)|\varphi_v(t)\rangle+\langle\varphi_v(t)|\partial_t\varphi_v(t)\rangle]\Delta t \tag{A5}$$

to first order in Δt. This already proves the relation, because the states $|\varphi_v(t)\rangle$ can be taken to be real. Therefore, $\partial_t|\varphi_v(t)\rangle=|\partial_t\varphi_v(t)\rangle$ can be expanded according to

$$|\partial_t\varphi_v(t)\rangle=\sum_{v'\neq v}^{\infty}|\varphi_{v'}(t)\rangle\langle\varphi_{v'}(t)|\partial_t\varphi_v(t)\rangle=\sum_{v'\neq v}^{\infty}\frac{|\varphi_{v'}(t)\rangle}{\varepsilon_v(t)-\varepsilon_{v'}(t)}\langle\varphi_{v'}(t)|\,\delta\dot{v}_{ee}|\varphi_v(t)\rangle. \tag{A6}$$

Insertion of our specific model for δv_{ee} [Eqs. (14),(15),(17)] yields

$$|\partial_t\varphi_v(t)\rangle=-\frac{\dot{P}_{\rm net}^{\rm loss}}{N-1}\left[1-\left(1-\frac{P_{\rm net}^{\rm loss}}{N}\right)^{N-1}\right]\times\sum_{v'\neq v}^{\infty}\frac{|\varphi_{v'}(t)\rangle}{\varepsilon_v(t)-\varepsilon_{v'}(t)}\langle\varphi_{v'}(t)|v_{ee}^0|\varphi_v(t)\rangle. \tag{A7}$$

If we use this equation together with Eqs. (1) and (28) for the asymptotic time-derivative of the net electron loss (16), we obtain

$$\dot{P}_{\rm net}^{\rm loss}|_{t\to\infty}=\frac{2\dot{P}_{\rm net}^{\rm loss}}{N-1}\left[1-\left(1-\frac{P_{\rm net}^{\rm loss}}{N}\right)^{N-1}\right]\times\sum_{i=1}^{N}\sum_{v=1}^{V}\sum_{v'>V}^{\infty}\frac{\langle\varphi_v(t)|v_{ee}^0|\varphi_{v'}(t)\rangle}{\varepsilon_v(t)-\varepsilon_{v'}(t)}\times{\rm Re}[c_v^{i}{}^*(t)c_{v'}^i(t)]|_{t\to\infty}. \tag{A8}$$

Note that the amplitudes $c_v^i(t)$ are now defined with respect to the states $|\varphi_v(t)\rangle$

$$c_v^i(t)=\langle\varphi_v(t)|\psi_i(t)\rangle. \tag{A9}$$

Equation (A8) can in general only be satisfied for

$$\dot{P}_{\rm net}^{\rm loss}|_{t\to\infty}=0, \tag{A10}$$

which according to Eq. (A7) proves Eq. (A2).

The key to the asymptotic stability is the fact that the time-dependence of the response potential (14) is driven by the net electron loss. Equation (A6) indicates that asymptotic couplings persist in more general situations, even though the analysis is performed in terms of the eigenfunctions of the asymptotic Hamiltonian. In contrast to the analysis with respect to the undisturbed atomic states $|\varphi_v^0\rangle$ [see Eq. (24)] the transition amplitudes are coupled via the time-derivative of the response potential δv_{ee} rather than by δv_{ee} itself.

[1] W. Fritsch and C. D. Lin, Phys. Rep. **202**, 1 (1991); F. Martín and A. Salin, Phys. Rev. A **55**, 2004 (1997); T. Bronk, J. F. Reading, and A. L. Ford, J. Phys. B **31**, 2477 (1998); G. Bent, P. S. Krstić, and D. R. Schultz, J. Chem. Phys. **108**, 1459 (1998); C. Pfeiffer, N. Grün, and W. Scheid, J. Phys. B **32**, 53 (1999).

[2] S. Suzuki, N. Shimakura, J. P. Gu, G. Hirsch, R. J. Buenker, M. Kimura, and P. C. Stancil, Phys. Rev. A **60**, 4504 (1999); P. C. Stancil *et al.*, J. Phys. B **31**, 3647 (1998); M. Kimura, J. P. Gu, G. Hirsch, and R. J. Buenker, Phys. Rev. A **55**, 2778 (1997).

[3] J. H. McGuire, *Electron Correlation Dynamics in Atomic Collisions* (Cambridge University Press, Cambridge, England, 1997).

[4] T. Kirchner, L. Gulyás, H. J. Lüdde, A. Henne, E. Engel, and R. M. Dreizler, Phys. Rev. Lett. **79**, 1658 (1997).

[5] T. Kirchner, L. Gulyás, H. J. Lüdde, E. Engel, and R. M. Dreizler, Phys. Rev. A **58**, 2063 (1998).

[6] T. Kirchner, H. J. Lüdde, and R. M. Dreizler, Phys. Rev. A **61**, 12 705 (2000).

[7] T. Kirchner, H. J. Lüdde, M. Horbatsch, and R. M. Dreizler, Phys. Rev. A **61**, 52 710 (2000).

[8] E. Engel and S. H. Vosko, Phys. Rev. A **47**, 2800 (1993); E. Engel and R. M. Dreizler, J. Comput. Chem. **20**, 31 (1999).

[9] H. J. Lüdde, A. Henne, T. Kirchner, and R. M. Dreizler, J. Phys. B **29**, 4423 (1996); O. J. Kroneisen, H. J. Lüdde, T. Kirchner, and R. M. Dreizler, J. Phys. A **32**, 2141 (1999).

[10] A. Henne, H. J. Lüdde, and R. M. Dreizler, J. Phys. B **30**, L565 (1997); T. Kirchner, H. J. Lüdde, O. J. Kroneisen, and R. M. Dreizler, Nucl. Instrum. Methods Phys. Res. B **154**, 46 (1999); T. Kirchner, M. Keim, A. Achenbach, H. J. Lüdde, O. J. Kroneisen, and R. M. Dreizler, Phys. Scr. **T80**, 270 (1999).

[11] J. -P. Blaizot and G. Ripka, *Quantum Theory of Finite Systems* (MIT Press, Cambridge, 1986), Chap. 9; P. Ring and P. Schuck, *The Nuclear Many-Body Problem* (Springer, New York, 1980), Chap. 12.

[12] E. K. U. Gross, J. F. Dobson, and M. Petersilka, in *Topics in Current Chemistry*, edited by R. F. Nalewajski (Springer, Heidelberg, 1996), Vol. 181, p. 81.

[13] W. Stich, H. J. Lüdde, and R. M. Dreizler, J. Phys. B **18**, 1195 (1985).

[14] A. Henne, A. Toepfer, H. J. Lüdde, and R. M. Dreizler, J. Phys. B **19**, L361 (1986).

[15] K. J. Schaudt, N. H. Kwong, and J. D. Garcia, Phys. Rev. A **43**, 2294 (1991).

[16] K. Gramlich, N. Grün, and W. Scheid, J. Phys. B **19**, 1457 (1986).

[17] P. Kürpick, W. -D. Sepp, H. J. Lüdde, and B. Fricke, Nucl. Instrum. Methods Phys. Res. B **94**, 183 (1994).

[18] R. Nagano, K. Yabana, T. Tazawa, and Y. Abe, J. Phys. B **32**, L65 (1999).

[19] C. Bottcher, Nucl. Instrum. Methods Phys. Res. B **10/11**, 7 (1985).
[20] W. Stich, H. J. Lüdde, and R. M. Dreizler, Phys. Lett. **99A**, 41 (1983).
[21] J. J. Griffin, P. C. Lichtner, and M. Dworzecka, Phys. Rev. C **21**, 1351 (1980); Y. Alhassid and S. E. Koonin, *ibid.* **23**, 1590 (1981).
[22] M. E. Rudd, T. V. Goffe, and A. Itoh, Phys. Rev. A **32**, 2128 (1985).
[23] R. D. DuBois, Phys. Rev. A **36**, 2585 (1987).
[24] L. H. Andersen, P. Hvelplund, H. Knudsen, S. P. Møller, A. H. Sørensen, K. Elsener, K.-G. Rensfelt, and E. Uggerhøj, Phys. Rev. A **36**, 3612 (1987).
[25] R. L. Becker, A. L. Ford, and J. F. Reading, Nucl. Instrum. Methods Phys. Res. B **10/11**, 1 (1985).
[26] K. C. Kulander, Phys. Rev. A **36**, 2726 (1987); *ibid.* **38**, 778 (1988).
[27] M. Horbatsch, Phys. Lett. A **187**, 185 (1994).
[28] H. J. Lüdde and R. M. Dreizler, J. Phys. B **18**, 107 (1985); P. Kürpick, H. J. Lüdde, W. D. Sepp, and B. Fricke, Z. Phys. D: At., Mol. Clusters **25**, 17 (1992).
[29] C. A. Ullrich, U. J. Gossmann, and E. K. U. Gross, Phys. Rev. Lett. **74**, 872 (1995).
[30] L. Gulyás (private communication).